Multiple Seed Waveform (MSW) Site Vibration Characterization – Signature Holes and Production Blasts, and Air Overpressure Estimate.

Ruilin Yang, Orica USA Inc
Lee Pratt, Orica Canada Inc.
April 2011

Executive Summary

A site characterization of blast vibration was conducted the Ajax property near Kamloops, B.C. for Abacus Mining and Exploration. Two sets of signature holes were fired. One set of signature holes was fired in the waste overburden, and the other set was fired in the ore body. The vibration and air over pressure from the blasts were monitored and analyzed. Two small production blasts were also fired during the monitoring. The site characterization information is to be used to design production blasts in order to manage blast vibration and air over pressure.

The site characterization information obtained includes:

1) Site vibration attenuation law from signature hole vibration for the waste rock and ore body respectively, as shown in Figures 17 and 18;

2) The ground sonic velocity is estimated to be 3200 m/sec for both waste rock, as well as the ore body.

3) Multiple seed waveforms were recorded at different distances for input to the Multiple Seed Wave (MSW) vibration modeling.

4) Using the above input data, the MSW model was used to predict the blast vibration from the two small production blasts and compared to the field measurements, as shown in Figures 25 and 26. The MSW model predicted the blast vibration at the city boundary (M9 in Figures 1 and 2) to be 1.26 mm/s and 0.79 mm/s respectively from the two small production blasts. Such predictions are valid for production blasts with a similar design as of the small production blasts (delay and charge weight per delay) and similar distance to the point of interest.

5) The measurement shows that the blast vibration measured on ground surface near the pipeline could provide a good estimate to the vibration on the pipeline (Table 3). The PPV on the exposed spot of the pipeline from the second small production blast was 5.98 mm/s.

6) The ground resonant frequency and the frequency range that the ground supports were estimated from the signature hole vibration, as shown in Figure 14 and Table 5. This information can be used to guide future production blast design to shift vibration frequency.

7) The peak air over pressure attenuation with scaled distance from signature holes was measured in a relatively calm weather (Figure 11). The attenuation law can be used to estimate air over pressure from production blasts. With the signature hole data, the Orica air over pressure model predicted the air over pressure at the city boundary to be 111 dB or 108 dB (Table 4) from the two small production blasts for a calm day.

8) The multiple seed waveforms recorded at different distances and the parameters from the analysis are input to the MSW blast vibration model. With the MSW modeling, various scenarios of blast design can be modeled and compared in terms of vibration control for peak particle velocity and frequency shifting.

9) For easy reference, Tables 6 and 7 show the predicted PPV from the two small production blasts versus the distance from a point of interest to the dominant charge in the blast. If a blast vibration limit is specified for a point of interest, for a give blast design, a table for the charge weight versus the distance can be built from the modelling.

10) The predicted PPV at the perimeter to surrounding cities around the mine (Table 8) is well below the vibration limit of 25.4 mm/s that is normally adapted by North America municipalities. The PPV is even well below human perception - 0.5 to 1.5 mm/s. The predicted air over pressure at the perimeter points (Table 9) is well below 120 dB that begins to cause complaints.

Introduction

Field work to characterize blast vibration was conducted at the Ajax property of Abacus Mining and Exploration on February 19, 2011. Two sets of signature holes were fired. One set of signature holes was fired in the overburden, and the other set was fired in the ore body. Each set of signature holes consists of seven single blast holes fired at 1.6 second intervals, followed by a small production blast with 8 blast holes fired with 20 ms hole-to-hole. Tri-axial blast vibration and air overpressure were recorded for signature hole blasts, as well as the small production blasts.

The signature hole vibration data has been used to build the site-specific vibration attenuation law. The vibration waveforms collected at different distances to signature holes were used as seed wave input to the Multiple Seed Waveform (MSW) blast vibration model. From the FFT analysis the power spectrum of the signature hole vibration is obtained. The power spectrum of the signature hole blast vibration indicates the ground resonant frequency and the frequency range of the blast vibration that the ground can support. This information is the basis for frequency shifting of production blast vibration.

The modeling using the MSW model is conducted with the signature hole data as input. The comparison between the modeled vibration and the measured vibration from the small production blasts is demonstrated. Future design scenarios of production blasts at the site can be modeled with the collected signature hole information as input.

Field Monitor Setup

The blast vibration monitoring is conducted with accelerators rather than the standard geophones typically used for compliance monitoring. Accelerometers are more suitable for critical vibration assessments as they do not experience the drawbacks of geophones in terms of amplitude and frequency range limitations. Accelerometers have much better low frequency sensitivity as compared to standard geophones. A more accurate measurement will better assist the operation in managing vibration response at points of interest or concern.

Table 1: Summary of monitors for Blast#1 (refer to Figure 1)

Monitor #	Record	Remarks
4	Tri-axial accelerometer	O.K.
5	Tri-axial accelerometer	O.K.
6	Tri-axial accelerometer	O.K.
7	Tri-axial accelerometer	O.K.
8	Tri-axial accelerometer and air over pressure	O.K.
9	Tri-axial accelerometer and air over pressure	Not triggered, 1230m from the blast
14	Tri-axial accelerometer	O.K.
15	Tri-axial accelerometer and air over pressure	O.K.

The plan views of the first and second blasts with monitor locations are shown in Figures 1 and 2. The monitors #6 and #8 and #9 were kept at the same location for both blasts. Monitor #8 and #9 were connected with both a microphone and a set of tri-axial accelerometers. Monitor #9 was placed at the city boundary and over 1230 meters away from the blasts. It was found that Monitor #9 was not triggered from both blasts due to the large distance from the blasts. Tables 1 and 2 summarize the monitors for the blasts.

Table 2: Summary of monitors for Blast#2 (refer to Figure 2)

Monitor #	Record	Remarks
1	Tri-axial accelerometer	O.K.
4	Tri-axial accelerometer	O.K.
5	Tri-axial accelerometer	O.K.
7	Tri-axial accelerometer	O.K.
8	Tri-axial accelerometer and air over pressure	O.K.
9	Tri-axial accelerometer and air over pressure	Not triggered, 1480 m from the blast
14	Tri-axial accelerometer	O.K.
15	Tri-axial accelerometer and air over pressure	On the top of the pipeline that is 10 feet deep from the ground surface and 15 feet away from Monitor#14 horizontally.

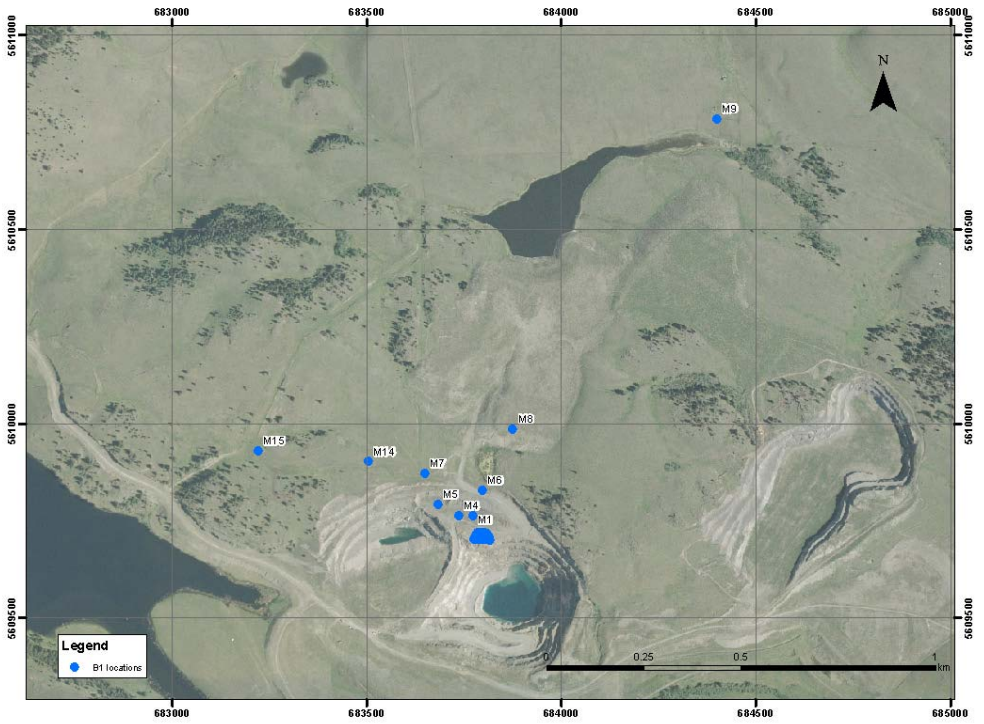

Figure 1. Blast and monitoring layout for the 1st blast on Feb 19, 2011

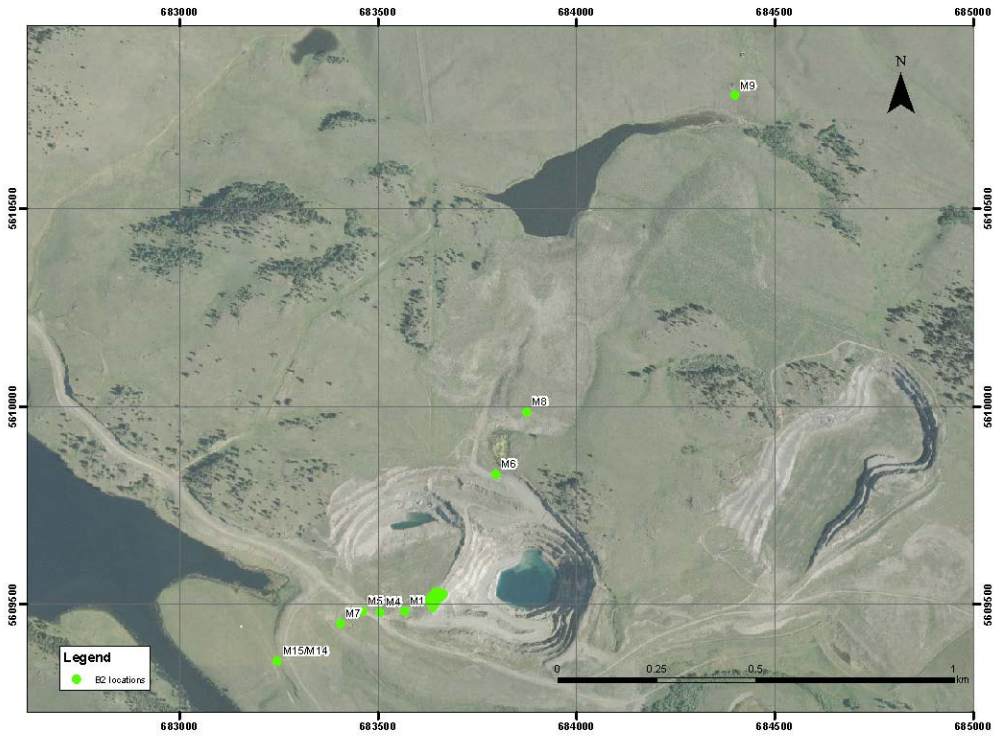

Figure 2. Blast and monitoring layout for the 2nd blast on Feb 19, 2011

Results of the Monitoring

Vibration on the Pipeline

There was a gas pipeline situated 440 m west from the second blast. One spot of the pipeline was uncovered and the top of the pipeline was exposed. The top of the pipeline was 3.5 m below the ground surface. During the second blast monitoring, one tri-axial sensor (Monitor 15) was fixed on the top side of a pipeline (Monitor 15 in Figure 4). The tri-axial sensor Monitor 14 (in Figure 3) was mounted on the surface of the ground. The two sensors were separated by 4.5 m horizontally. Figures 3 and 4 show the recorded tri-axial acceleration traces with the sensor Monitor 14 and Monitor 15 from the second blast. The second blast consisted of seven signature holes (separated by 1.6 s) and a small production blast. The small production blast was fired 1.6 second after the seventh signature hole. The vibration from the small production blast is the eighth wavelets in Figures 3 and 4. The small production blast had two rows. Each row included four blast holes. The hole-to-hole delay was 20 ms and the delay between rows was 110 ms. By integrating the acceleration traces the particle velocity traces were obtained.

Table 3 compares the peak particle acceleration (PPA) and velocity (PPV) recorded by sensor Monitor 14 (on the ground surface) and the sensor Monitor 15 (on the pipeline). It can be seen that both peak particle acceleration and velocity measured on the pipeline could be slightly lower or higher than those in the ground surface. However, the vibration measured on the pipeline is very much comparable to that on the ground surface. The small variation could be partly due to the difference in the sensor mounting.

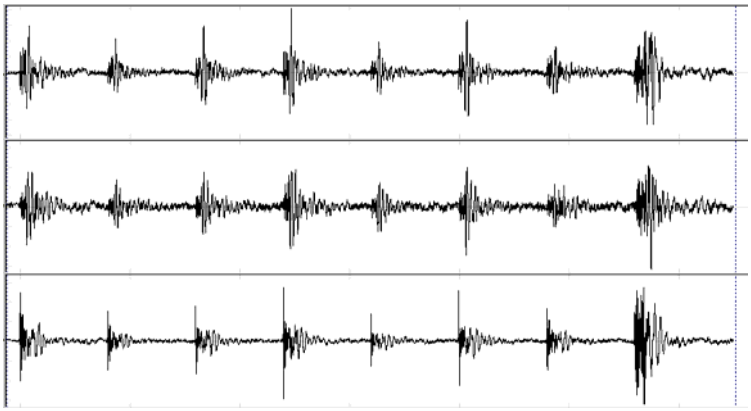

Figure 3. Tri-axial acceleration traces from Monitor 14 (on ground surface near pipeline) on the second blast

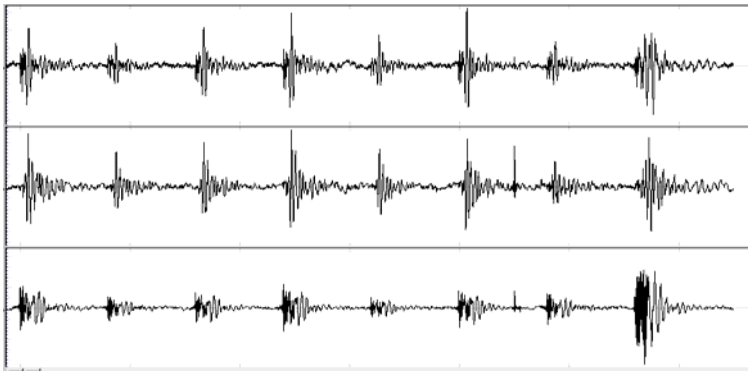

Figure 4. Tri-axial acceleration traces from Monitor 15 (on pipeline) on the second blast

Table 3. Peak particle acceleration (PPA) and velocity (PPV) recorded with Monitors 14 and 15

Blast hole #	Sensor #14 - the ground surface, PPA (g)	Sensor #15 - the pipeline , PPA (g)	Sensor #14 - the ground surface, PPV (mm/s)	Sensor #15 - the pipeline , PPV (mm/s)
1	0.056	0.059	3.51	3.66
2	0.035	0.025	1.99	2.02
3	0.042	0.034	3.45	2.78
4	0.064	0.058	3.66	3.60
5	0.030	0.026	2.02	2.10
6	0.058	0.045	3.16	3.49
7	0.035	0.031	1.91	1.66
8-15 (mini production blast)	0.073	0.11	6.29	5.98

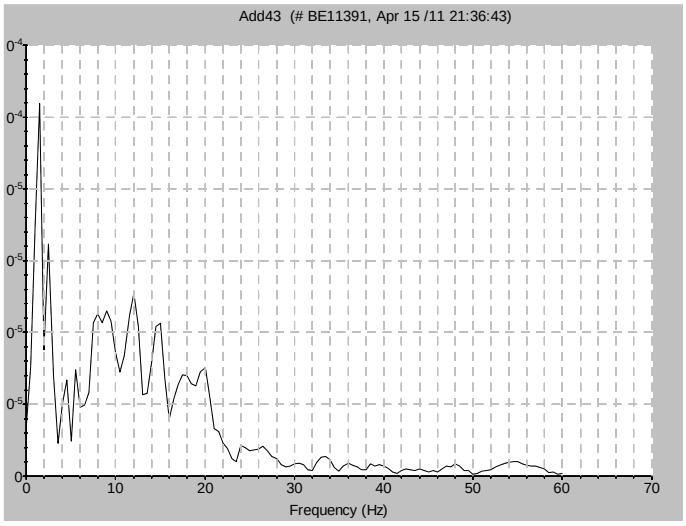

Figure 5. Amplitude spectrum of vibration on ground surface from Signature Hole #6

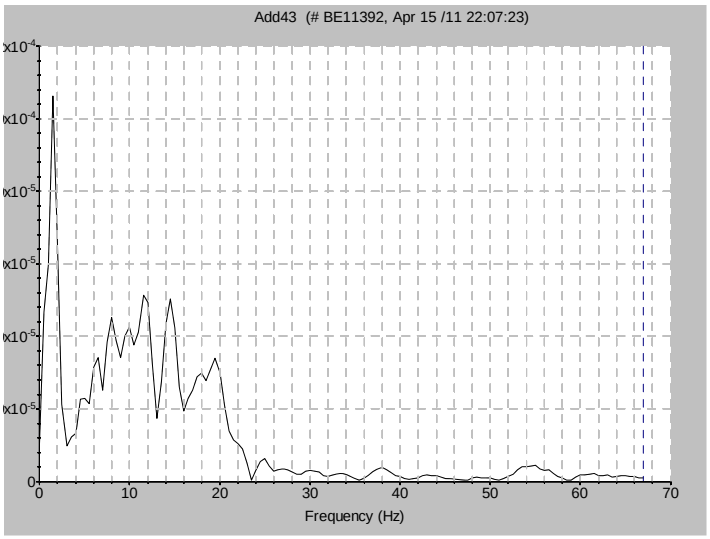

Figure 6. Amplitude spectrum of vibration on pipeline from Signature Hole #6

Figures 5 and 6 are amplitude spectrums of the vibration recorded respectively with Monitor #14 and Monitor #15 from the signature hole #6 in the second blast. From both the Figures it can be seen that peaks are at 1.5 Hz and 12 Hz. Secondly, there is not much vibration beyond 60 Hz in both the graphs. Most significant vibration energy is below 30 Hz. Therefore, the frequency response of the pipeline seems similar to that of the ground. Therefore, blast vibration measured on ground surface near the pipeline could provide a good estimate to the vibration on the pipeline.

Air Over Pressure

Monitors #8 and #9 were placed at the same spots without relocation for both Blast #1 and #2. Both monitors contained a set of tri-axial accelerometer and a microphone. Since Monitor #9 was 1230 m from the first blast and 1480m from the second blast, it was not triggered from neither of the blasts due to the large distances. The trigger level for the air over pressure was 115 dB and the trigger level for the blast vibration was 0.08 g. However, Monitor #8 recorded both vibration and air over pressure from the two blasts. The records from Monitor #8 for the 1st and 2nd blast are displayed in Figures 7 and 8, respectively. In both figures, the records in the Channels #1, #2, and #3 are the tri-axial accelerations of the ground and the record in the Channel #4 is the air over pressure signals. The vibration and the air over pressure signals are generated from the signature holes (Hole #1 - #7) followed by the signals from the small production blasts (Holes #8 - #15).

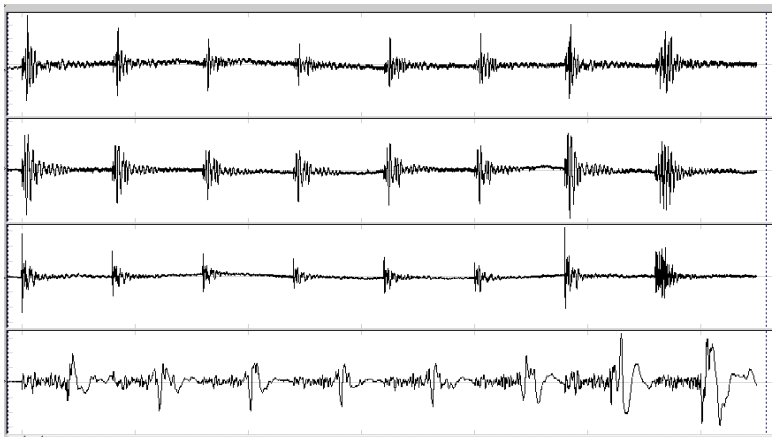

Figure 7. Records from Monitor #8 in 1st Blast – Channel #1-3 ground acceleration and Channel #4 air over pressure

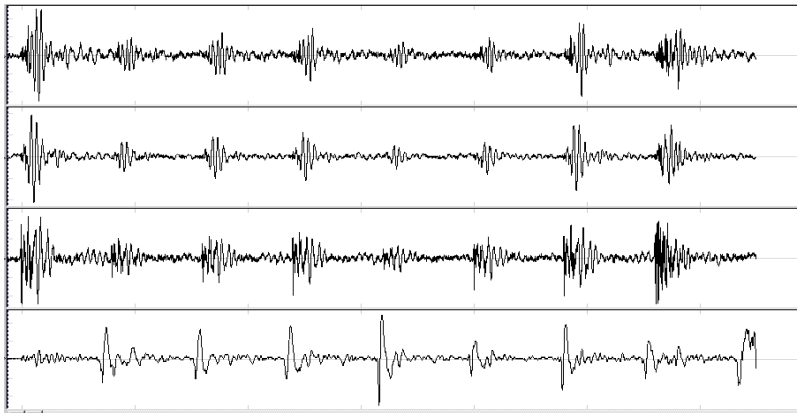

Figure 8. Records from Monitor #8 in 2nd blast – Channel #1-3 ground acceleration and Channel #4 air over pressure

From the signals in Channel #4 in Figures 7 and 8, the air over pressure from each signature hole can be clearly identified. As it is seen, an air over pressure signal from a signature hole has a positive peak and a negative peak. Both the positive and negative over pressures could be a disturbance to environment. Figure 9 shows a plot of peak air over pressure (the peak of the absolute pressure values) versus the square-root scaled distance. Figure 10 shows the pressure versus the cube-root scaled distance. The two plots are similar and no improved correlation can be seen between the two plots. From the figure the maximum air over pressure is 115.2 dB from the first set of the signature hole blasts (267 m to the monitor). The maximum pressure level from the second set of the signature hole blasts is 113 dB (520 m to the monitor). The pressure is scatter in a range of 8 dB, that could be due to the confinement, such as stemming or overburden of blast holes. The wind during the day was negligible when the blasts were fired.

Figure 11 shows regression curves of peak over pressure in psi versus the square root scaled distance since pressure in psi can be added directly and it is convenient for superposition of the pressure from different blast holes in a production blast. The regression equations in Figure 11 are valid for the attenuation of peak over pressures from signature hole blasts and it can be used as the model input to model air overpressure from production blasts.

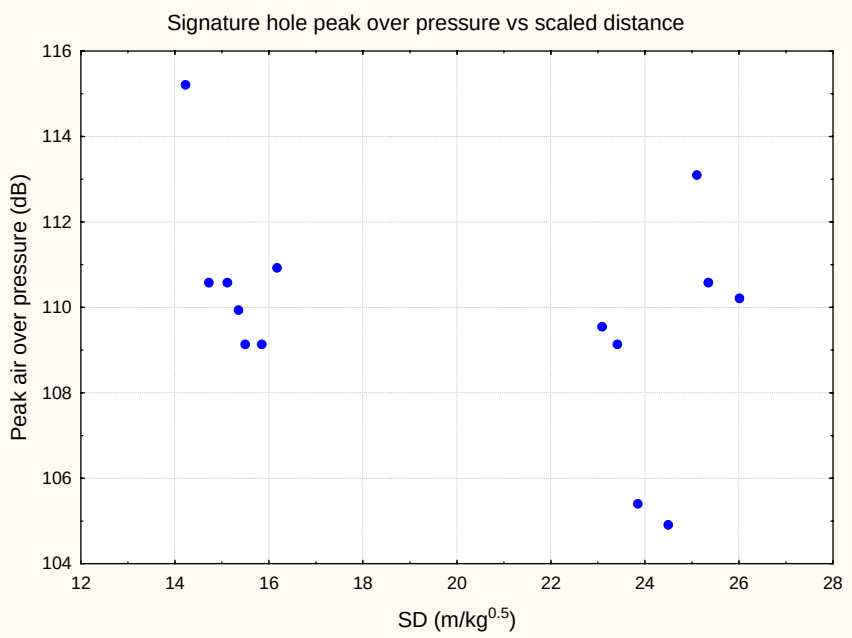

Figure 9. Peak pressure versus the square-root scaled distance for signature blast holes

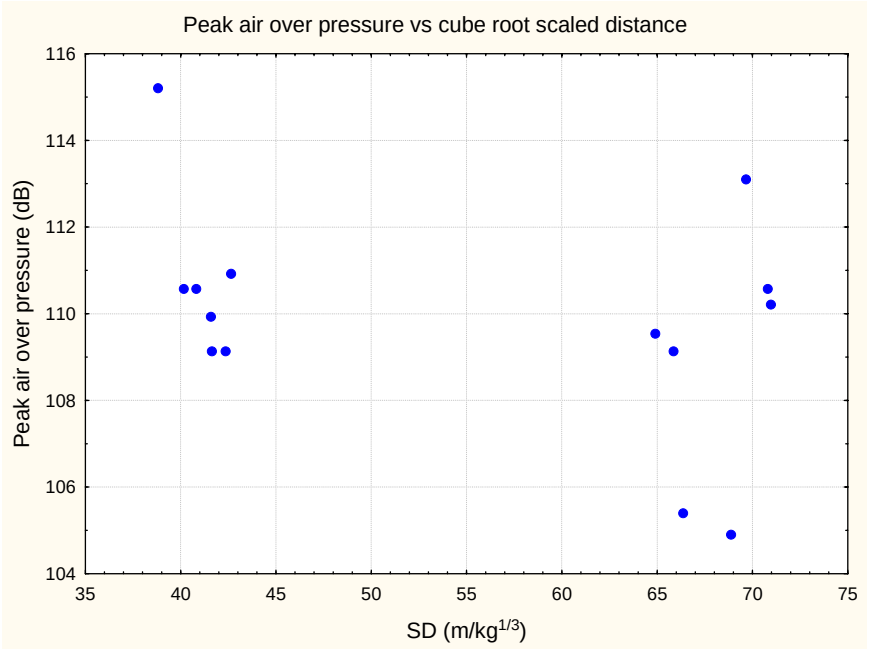

Figure 10. Peak pressure versus the cube-root scaled distance for signature blast holes

Orica Air Over Pressure Modeling

Orica has developed an air over pressure model based on multiple air over pressure signals from signature hole blasts and the attenuation law, such as that in Figure 11, to model the air over pressure from a production blast. Table 4 shows the predicted air over pressure at Monitor #8 (refer to Figures 1 and 2 above). The predicted air over pressure from the two small production blasts at Monitor #8 is compared with those measured. From the table, it can be seen that the model predicts the air over pressure at the Monitor #8. The air over pressure at Monitor #9 was low and it did not trigger the monitor. The air over pressure at Monitor #9 is predicted to be 111 dB and 108 dB respectively from

the first and the second production blasts. The model slightly over predicted the air over pressure at Monitor #9.

Table 4. Air over pressure prediction for the two small blasts at Monitors #8 and #9

Blast	Monitor	Measured (dB)	Predicted (dB)
1	#8	114	114
1	#9	Not triggered, due to low over pressure	111
2	#8	107	112
2	#9	Not triggered due to low over pressure	108

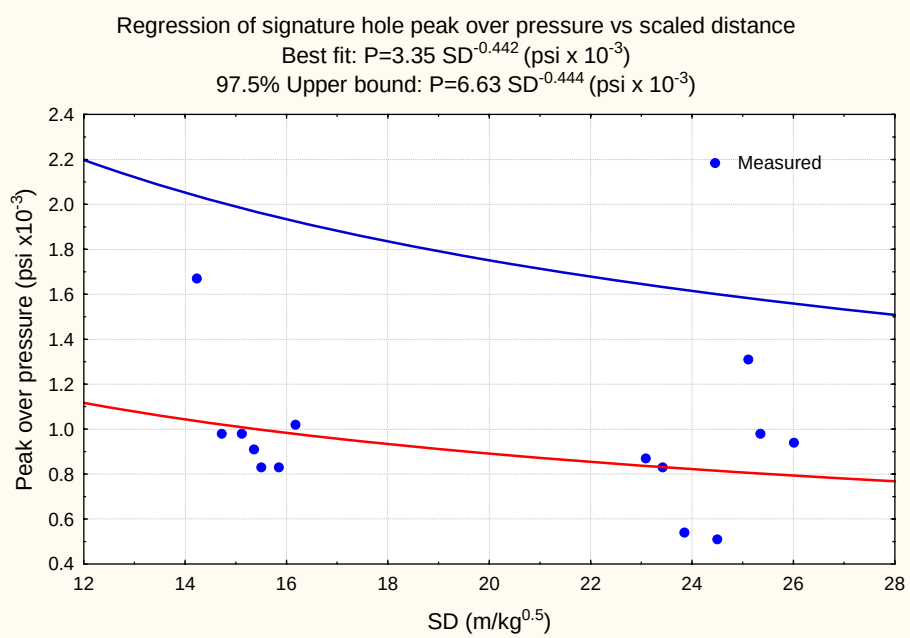

Figure 11. Regression curves and equations for the peak over pressure attenuation from the signature hole blast

Ground Sonic Velocity

An estimate of the ground sonic velocity is required for accurate modeling of blast vibration. The ground sonic velocity can be estimated from the time difference of the arrivals of the vibration signal and the air blast signal and the respective travel distance and the sound speed in the air. The time difference of the arrivals of the vibration and the air blast signals can be assessed from the signals of vibration and air over pressure recorded in separate channels of a seismograph, as shown in Figure 12. The weather condition at the time of the blasts was clear and little or no wind. The key factor affecting the sonic velocity in the air is temperature. The temperature was estimated to be around -5^{o} C. It was estimated the sonic speed in the air to be 328.26 m/s. From the analysis in Appendix A, the ground sonic velocity is estimated to be 3210 m/s from the first blast and 3199 m/s from the second blast. The difference in the ground sonic velocity from the two blasts is small.

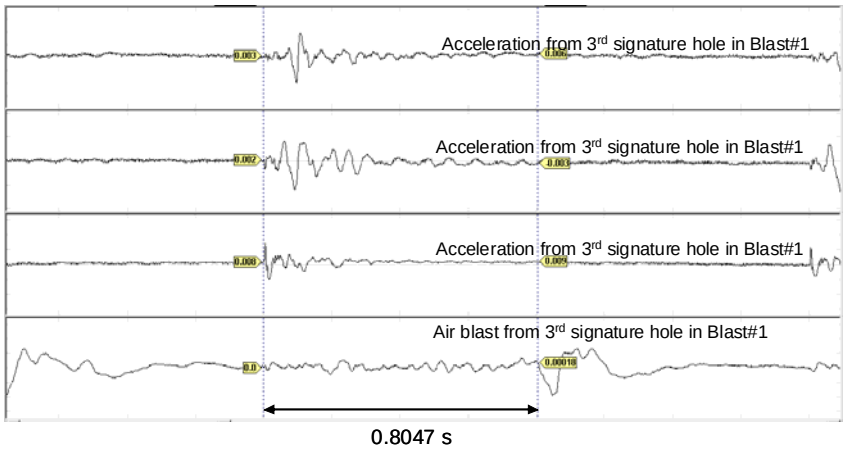

Figure 12. Arrival time difference between blast vibration (Channel #1-3) and air over pressure (Channel #4)

Seed waveforms

Figure 13 shows some waveforms of the vertical component of signature hole vibration recorded at different distance from the signature holes. It can be seen that the waveform change with the distance from signature holes is significant. With an increase of the distance from the signature hole to the monitor, the vibration waveform becomes more complex and longer duration due to addition of different wave types, such as shear and surface waves. Such an observation validates the necessity of using multiple seed waveforms to model blast vibration at a point of interest from a production blast.

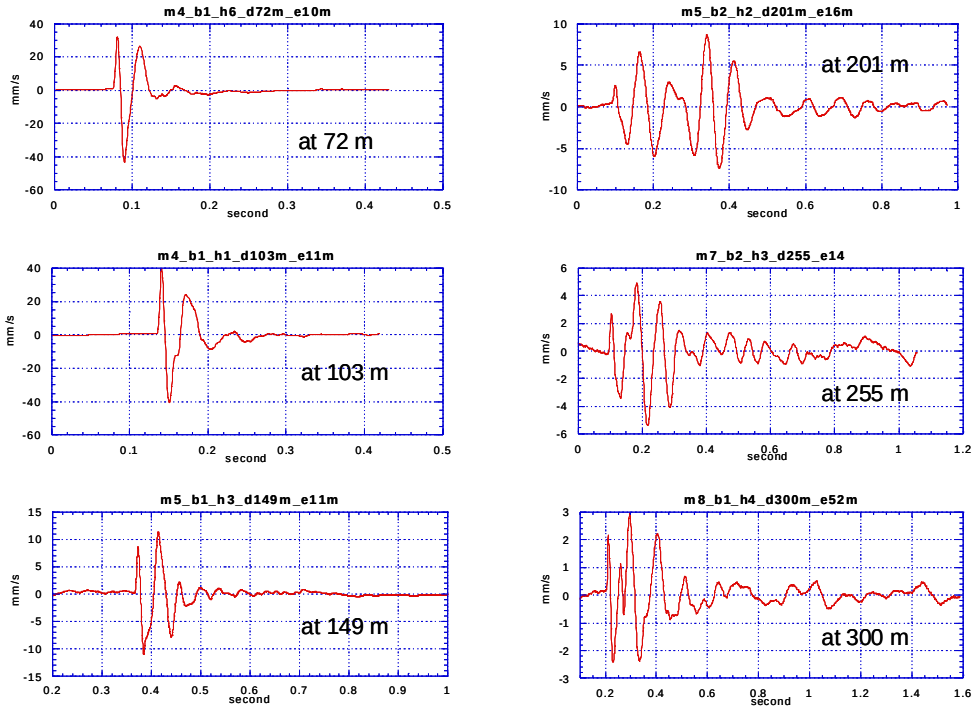

Figure 13. Waveforms of signature hole blast vibration measured at different distances from the blast hole

Ground frequency response at different distances to the signature hole

Figure 14 shows average spectrums of the tri-axial components of the vibration from the signature hole blasts at different distances. At 72 m from the signature hole, the significant blast vibration is over a frequency range of 0 - 75 Hz. The range becomes smaller when the distance from the blast hole becomes larger. At 513 m, there is no significant blast vibration beyond 20 Hz. The dominant frequency of the signature hole vibration at a given distance range can be considered as the resonant frequency of the ground (refer to the Appendix A). For example, at 72 m, the resonant frequency of the ground can be considered to be 24 Hz and at 513 m, it is 10 Hz. The peaks within 1 Hz to 2 Hz could be due to the slow motion of the ground and to be avoided obviously in design of production blasts since the vibration at lower frequency is more damaging to structures. The frequency range of the signature hole vibration can be considered as the frequency range that the ground can support. For example, at 149 m, the ground could support vibration up to 55 Hz. This means that potentially the dominant frequency from a production blast could be shifted to any frequency below 55 Hz through designing delay timing using electronic initiation. A successful frequency shifting from a production blast can only occur when the targeted dominant frequency to shift to is within the range that the ground supports (refer to Appendix B). Table 5 lists an estimate of the ground resonant frequencies and the frequency ranges that the ground supports. The information can be used as a reference for frequency shifting.

Table 5. Estimate of ground resonant frequency and frequency range that ground supports

Distance (m)	Resonant frequency (hz)	Range of frequency that the ground support (Hz)
70	1-3, 22-26	0 - 75
140	1-3, 20-24	0-55
200 - 300	1-3, 10-18	0-30
400	1-3, 7-13	0-25
500	8-12	0-18

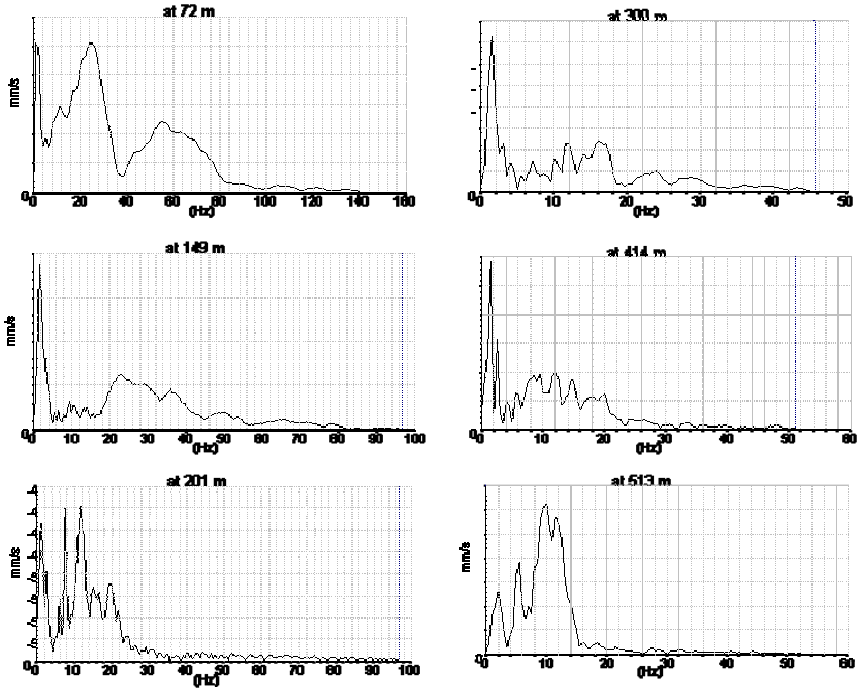

Figure 14. Amplitude spectrum of signature hole blast vibration at different distances from the blast hole

Site Attenuation Law of Peak Particle Velocity (PPV)

The site vibration attenuation can be characterized by the relationship between the PPV and the charge weight scaled distance of signature hole blast vibration since the signature hole vibration is not affected by blast delay timing among blast holes, such as in a production blast. For each of the two test blasts, a total of 49 data points were obtained from the signature hole blasts. Figure 15 shows the PPV versus the charge weight scaled distance of the signature hole blasts for the blasts in Figures 1 and 2. Figure 16 shows the PPA (peak particle acceleration) versus the charge weight scaled distance for the two blasts. Both Figures 15 and 16 show lower vibration amplitudes in the near field from the second blast than the first blast in the near field. This indicates the ground in the second blast (in the ore body) attenuates more blast vibration and the rock could be more fractured or weaker in strength than that of the first blast (in the overburden rock). The difference in the results confirms the necessity to conduct separate tests of the signature hole blast vibration for the two regions of geologies to establish an accurate site law for each site, respectively.

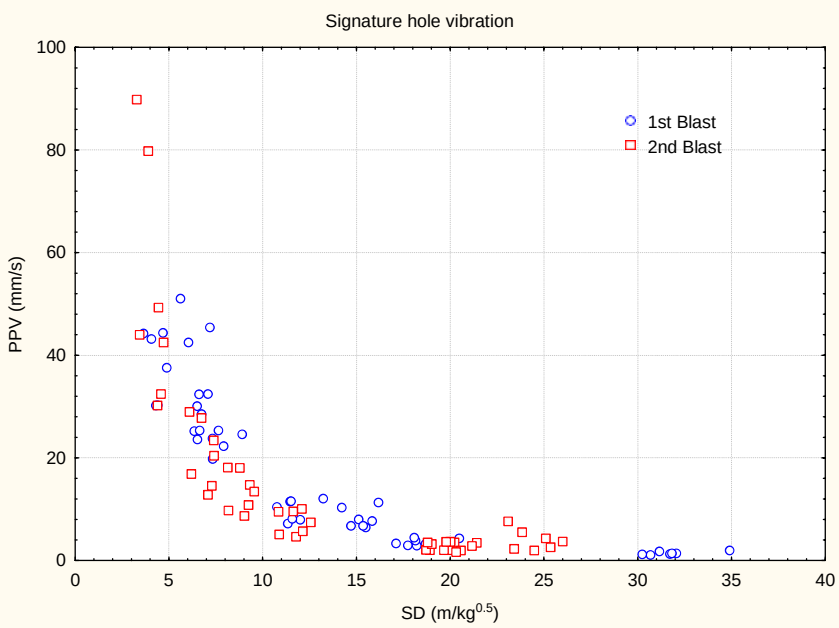

Figures 15. PPV versus the charge weight scaled distance of the signature hole vibration

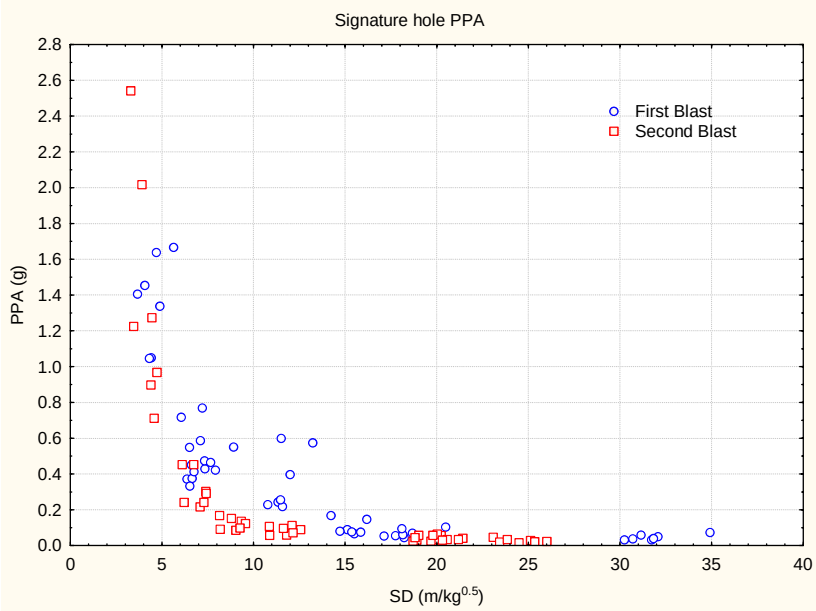

Figures 16. PPA versus the charge weight scaled distance of the signature hole blast vibration for the blasts in Figures 1 and 2.

Figures 17 and 18 show the regressions of the PPV against the scaled distances for the first and second signature hole blasts. The parameters of the regression equations will be a part of the input to the MSW blast vibration model for vibration modeling of production blasts.

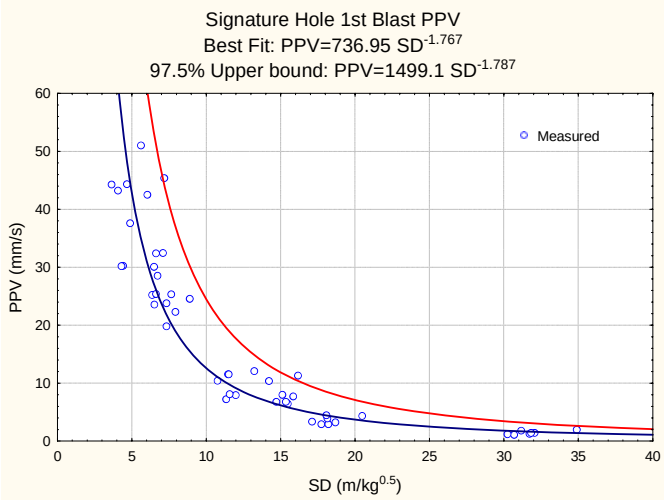

Figure 17. Regression of the PPV against the scaled distance for the first blast

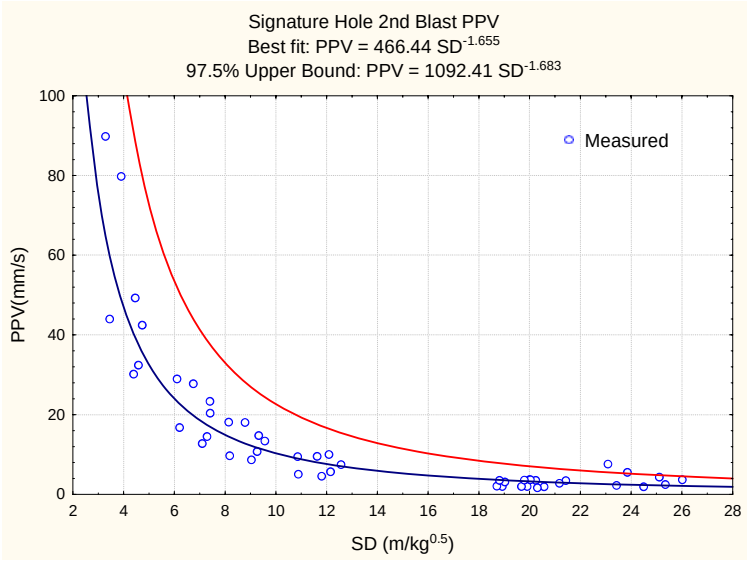

Figure 18. Regression of the PPV against the scaled distance for the second blast

Small Production Blasts

In vibration analysis, a basic requirement is to express peak particle velocity (PPV) or peak particle acceleration (PPA) in correlation with charge weight scaled distance. For a single hole blast, it is simple to determine the contributing charge weight and distance for a vibration peak value. However, for a production blast with multiple blast holes, the process of determining the contributing charges for a peak vibration value is more complex.

In reality, multiple blast holes contribute to a peak vibration value (PPA or PPV). However, field data from different sites show that PPA and PPV have a strong correlation with the minimum charge weight scaled distance. This implies there is a dominant charge for the PPV value at a specific monitoring location. This dominant charge is the one associated with the minimum scaled distance. Consequently, for near-field vibration monitoring the distance and charge weight of each blast hole must be examined for correlation with vibration measurement. The minimum charge weight scaled distance (MSD) can be defined as:

$$MSD = \min\left(\frac{d_1}{\sqrt{w_1}}, \frac{d_2}{\sqrt{w_2}}, ..., \frac{d_n}{\sqrt{w_n}}\right) \quad (3)$$

where n is the total number of charges in the production blast, d_i is the distance from the i^{th} charge to the monitor, w_i is the charge weight of the i^{th} charge (Yang, 2007). When the above analysis is applied to far field vibration analysis, the MSD above approaches the scaled distance from the maximum charge in the blast pattern.

One small production blast was fired following the signature hole blasts in both the waste and ore body. Figure 19 shows the PPV from the two small production blasts versus the minimum scaled distance. For each blast, there are only seven PPV that were recorded with seven monitors. With limited data, no clear difference was observed for the PPV from the two production blasts.

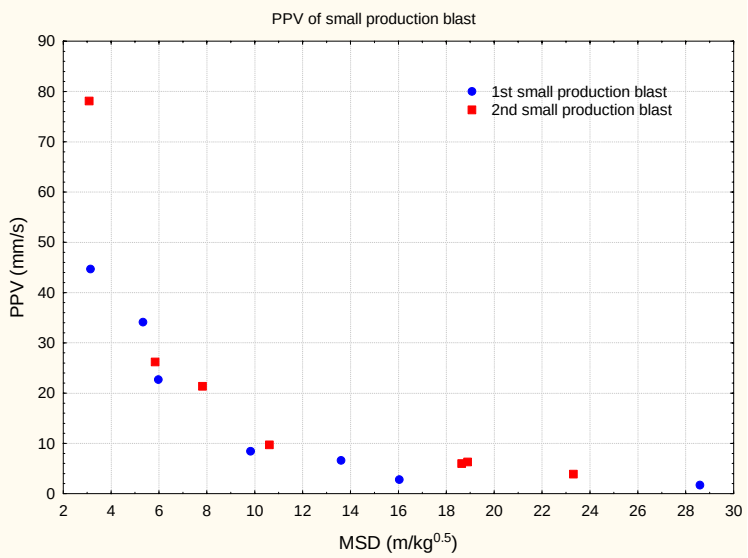

Figure 19. PPV from the two small production blasts versus the minimum scaled distance

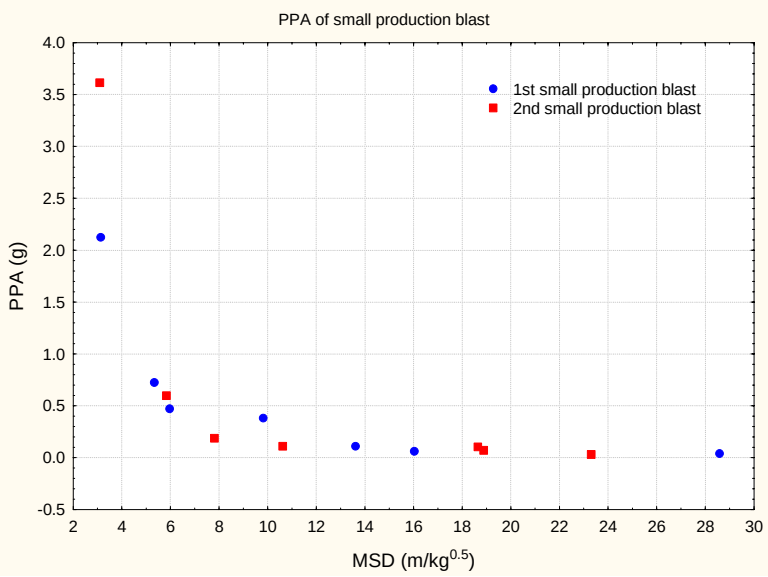

Figure 20. PPA from the two small production blasts versus the minimum scaled distance

Figure 20 shows the PPA from the two small production blasts versus the minimum scaled distance. Again with limited data, no clear difference was observed for the PPA from the two production blasts.

The Multiple Seed Waveform (MSW) Blast Vibration Model

The MSW model has been used for open pit coal mines with soft ground (Yang et al, 2008), hard rock quarries (Yang and Scovira, 2009), open pit gold/copper mines, oil sand blast, and underground tunnel blasting, for all the cases yielding reliable predictions. The reliable prediction for the wide range of applications is based on the capability of the model components that simulate the major treads of the blast vibration for various applications. The major components of the model have been reported in previous papers (Yang and Scovira, 2010).

Using Multiple Seed Waveform as Input

In contrast to most existing blast vibration models, the MSW model uses multiple sets of seed waveforms (Figure 21) and transfer functions to model how the vibration waveform changes from different blastholes to particular points of interest (Figure 22). Based on signature blasthole information at a site, the model can make reliable predictions. The concept of the MSW model is suitable for both near and far-field blast vibration predictions (Yang and Scovira, 2010).

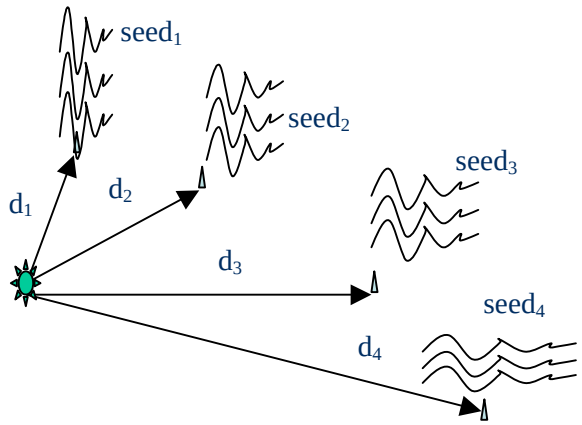

Figure 21. A sketch of multiple sets of seed waveforms measured at different distances from a signature hole

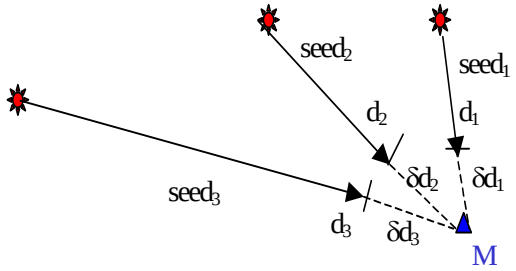

Figure 22. A set of signature waveforms is selected for each charge according to the distance match – multiple sets of seed waves used at a point of interest

By employing multiple seed waveforms, p-, s-, and surface waves from charges at different distances can be included in the model. Waveform changes in amplitude, frequency, and duration due to the mixture of wave types and frequency attenuation with distance are automatically taken into account by the multiple seed waveforms. In addition, some geological effects on different seed waveforms are also input to the model.

Screening Effect of an Earlier Firing Hole on Vibration from a Later Firing Hole

The MSW model takes into account the screening effect of broken ground from earlier firing holes within the same blast in the path of the vibration. The screening effect on both amplitude and waveform change from a blast hole are modeled in the MSW model. In addition, the screen algorithm in the MSW model simulates effects of the location and initiation time of an earlier firing charge in the path area of the vibration from a presently-firing hole. Figure 23 shows the path area of the vibration from the presently-firing hole and the location (d and c) and the advanced time (Δt) of a later firing hole (Yang and Kay, 2011) the effect of which are modeled in the MSW model.

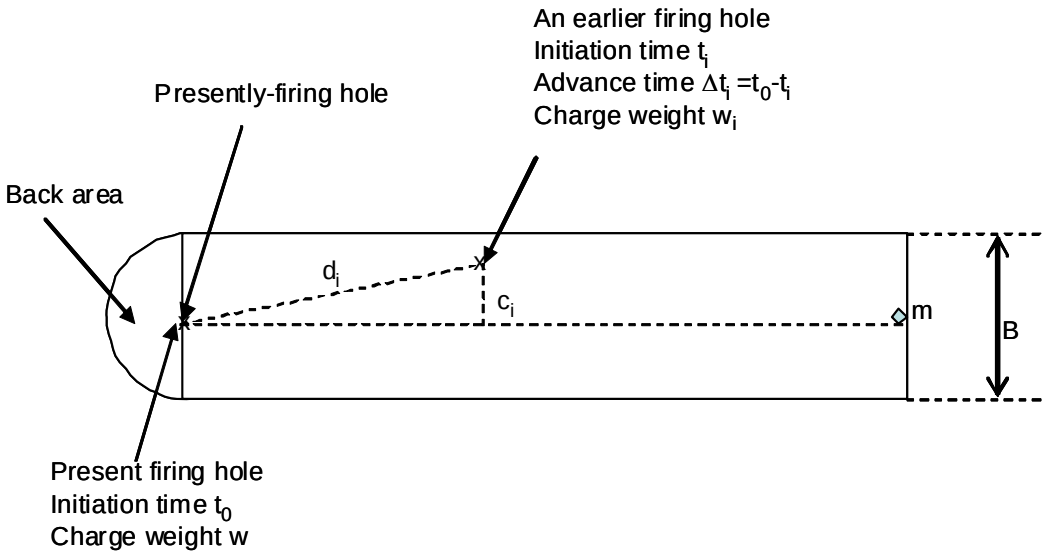

Figure 23. Path area where the earlier firing charges are accounted for screening the blast vibration from the presently-firing hole

Change of the Ratio Among the Tri-axial Components Due to Distance

From blast vibration monitoring, it is commonly observed that the vertical component is largest among the three components if the monitor is placed on the ground surface near a blast hole. Whereas, the radial component is largest if the monitor is placed far away (e.g. the distance is much larger than the depth of the blast hole) from blast holes. Such phenomenon of the blast vibration is modelled in the MSW model by three dimensional coordinate transformations on the tri-axial components of seed waveforms (Yang and Scovira, 2010). Figure 24 shows that the MSW model simulates that a further hole contributes more to the horizontal component and a closer hole generates more vertical component. Many applications have vibration limit specified in separate components. It is therefore necessary to model each component accurately.

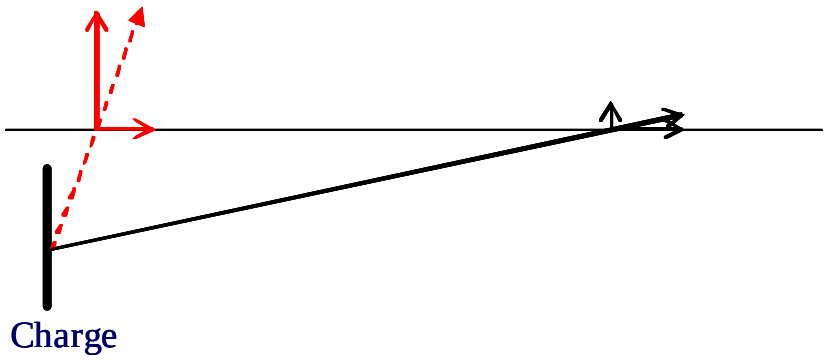

Figure 24. Change of the ratio among tri-axial components with distance that the MSW models

Statistical Modeling of Random Variable of Normal Distribution (Yang and Lownds, 2011)

Some variables involved in blast vibration are better modeled as random variables in a blast vibration model. For example wave propagation speed from a blasthole to a monitoring point often varies at the same site. The geological effect of the ground on the attenuation of the vibration amplitude also demonstrates variations such as the best-fit and 97.5% upper bound curves in Figures 17 and 18. The time delay of a detonator deviates from its nominal timing and it is thus realistic to model this as a random variable using a statistical approach. The MSW blast vibration model implemented statistical modeling including site vibration attenuation, ground sonic velocity, and timing delay scatter. The statistical modeling is based on the analysis of the field data in terms of their means and standard deviations (Yang and Lownds, 2011).

MSW Model Prediction vs. Measurement

The seed waveforms measured at different distances, the site attenuation parameters from the signature hole analysis in Figures 17 and 18, and the site sonic velocity are input to the MSW model to simulate the blast vibration at the monitoring points for the mini productions blasts from the waste rock and the ore body. Figure 25 shows the comparison between the model predicted and the measured PPV for the first mini production blast. At the nearest monitor, it seems that the model over predicts the blast vibration. This could be partly due to the limited number of measurements that could be lower than the actual trends (refer to Figure 25). At the rest of the monitors, the model yields reasonable predictions.

Figure 26 shows the comparison between the predicted and the measured PPV for the second production blast. At the second nearest monitor, it seems that the model over predict the blast vibration. In general, the model yields reasonable predictions. Slight over-prediction to the measurement provides a safety margin to use the model. The two data points between the scaled distances 18 and 20 in Figure 26 are the points on the pipeline and the ground surface near the pipeline spot. The model predicts the vibration at the pipeline.

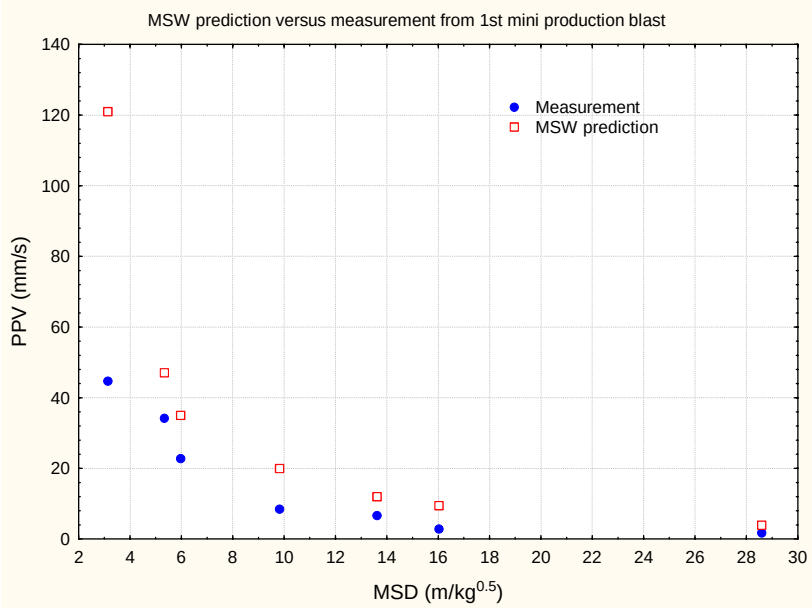

Figure 25. MSW prediction versus measurement from 1st small production blast

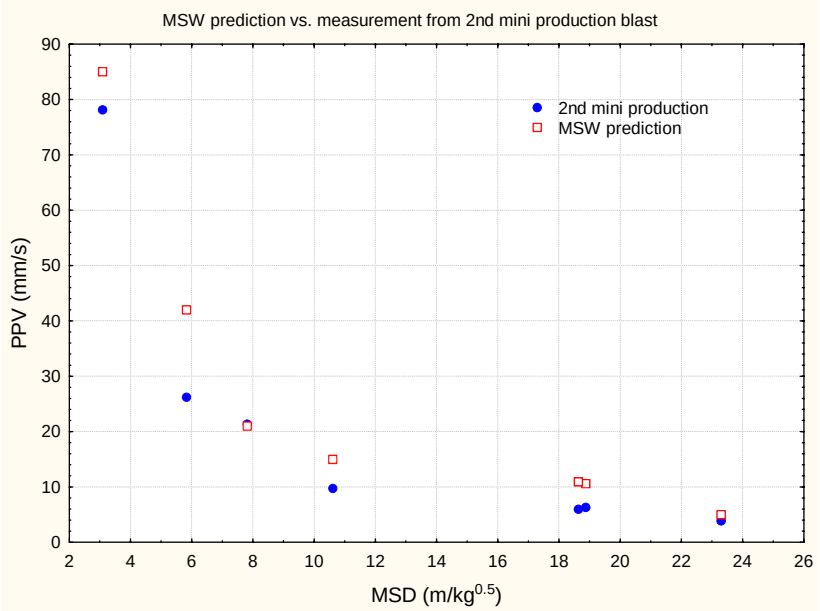

Figure 26. MSW prediction versus measurement from 2nd small production blast

As demonstrated in Figures 25 and 26, with the input of the signature hole vibration information, the model yields reasonable predictions to the production blast vibration. The model predicts that the PPV at Monitor #9 (near the city boundary) is 1.26 mm/s from the first small production blast and 0.79 mm/s from the second small production blast.

For easy reference, Tables 6 and 7 show the predicted PPV from the two small production blasts versus the distance from a point of interest to the dominant charge in the blast (refer to the above section on the minimum scaled distance – Equation 3).

Table 6. Predicted PPV from the first small production blast versus the distance to the nearest blast hole

Distance (m)	66	112	126	206	286	337	400	495	602
PPV (mm/s)	121	49	36	20	13	10	6.5	4.23	3.8

Table 7. Predicted PPV from the second small production blast versus the distance to the nearest blast hole

Distance (m)	67	127	170	232	302	406	412	515	596
PPV (mm/s)	86	41.7	21	15.4	9.02	11	10.5	5.5	3.55

For different blast design scenarios, similar tables can be generated as the above. If a blast vibration limit is specified for a point of interest, for a given blast design (timing and loading for each blast hole, hole depth and stemming, spacing and burden), a table for the charge weight versus the distance to the point of interest can be built from the modelling.

The model could provide predictions for different design scenarios. Comparison of prediction results could assist to identify improved and novel blast designs to provide blast vibration compliance and at the same time maximising the blasting productivity.

Model Prediction of PPV and Blast over Pressure for Points of Perimeter of Concern

The environmental and community reviewers expressed interest to know what the model PPV and noise overpressure would be at a total of 19 points signifying the perimeter to surrounding cities around the mine. Figure 27 shows the two small production blasts (fired on Feb 19) and the perimeter points, which are numbered from 1 to 19. Although the distance from the centre of the two blasts is about 230 m, the two production blasts appears to be very close due to the scale of the figure. Distances from the two small blasts to the points range from 2800 m to 9000 m.

Table 8 summarizes the predicted PPV from the two small production blasts. It can be seen that the blast vibrations at the perimeter points are well below the vibration limit of 25.4 mm/s that is normally adapted by North America municipalities. The predicted PPV is even well below human perception - 0.5 to 1.5 mm/s PPV. Table 9 shows the predicted air over pressure at all the perimeter points from the two small blasts. Again, the predicted over pressure is well below 120 dB that begins to cause complaints (Persson et al, 1994).

Table 8. Predicted PPV at 19 points signifying the perimeter to surrounding cities

Points #	PPV (mm/s) from Blast#1	Distance to Blast#1 (m)	PPV (mm/s) from Blast#2	Distance to Blast#2 (m)
1	0.085	3026	0.3	2820
2	0.050	3677	0.03	3929
3	0.010	5040	<0.01	5421
4	0.054	3371	0.09	3483
5	0.153	2365	0.39	2218
14	0.022	4532	<0.01	4284
The other points	< 0.01 mm/s		< 0.01 mm/s	

Table 9. Predicted air over pressure at 19 points signifying the perimeter to surrounding cities

Points #	Over pressure from Blast#1 (dB)	Distance to dominant hole of Blast#1 (m)	Over pressure from Blast#2 (dB)	Distance to dominant hole of Blast#2 (m)
1	110.7	3026	112.3	2820
2	113.6	3677	115.3	3929
3	113.6	5040	113.6	5421
4	113.6	3371	113.6	3483
5	108.2	2365	111.5	2218
6	110.7	8490	112.3	8576
7	112.3	7325	113.6	7495
8	113.6	6336	114.2	6565
9	114.2	6389	114.2	6640
10	113.6	7006	113.6	7227
11	113.6	7399	113.6	7547
12	113.0	6667	108.4	6743
13	112.3	5911	112.7	5847
14	108.5	4532	108.8	4284
15	108.1	7324	108.1	7089
16	109.5	7795	108.8	7603
17	108.9	8682	110.3	8552
18	109.5	9139	110.7	9076
19	110.2	9816	111.5	9820

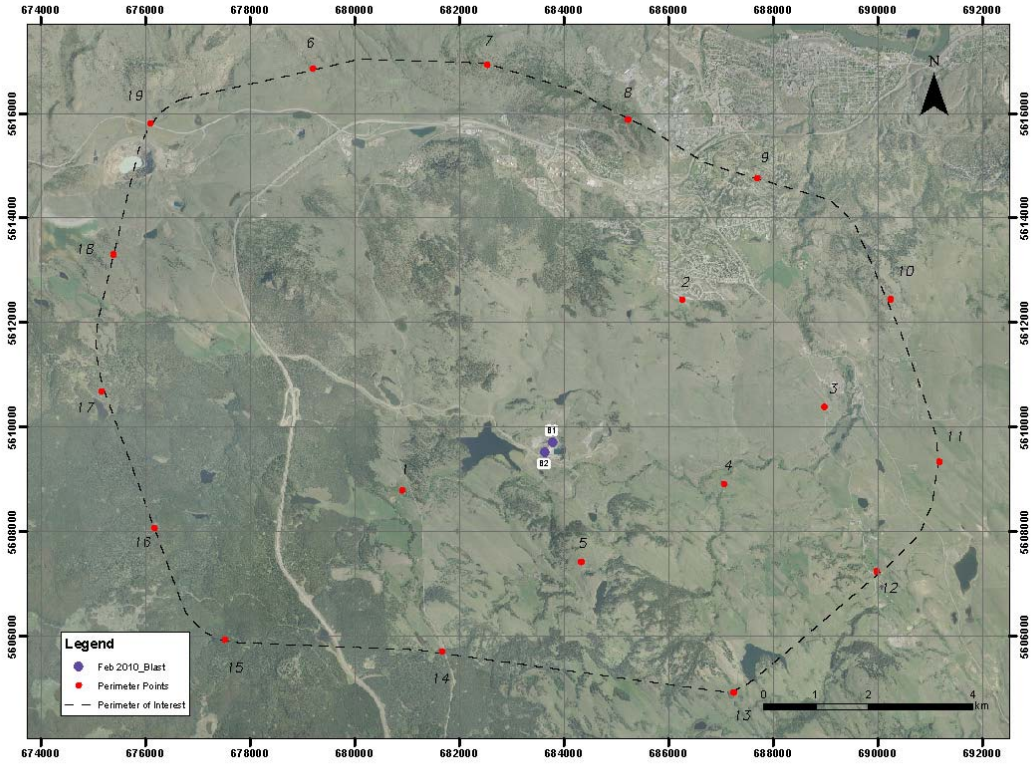

Figure 27. Two small production blasts (fired on Feb 19) and the perimeter points numbered from 1 to 19

Conclusions

Site vibration characterization has resulted in useful information for future blast design and modelling in terms of controlling blast vibration in the high walls or nearby pipeline, as well as air blast estimation.

Recorded air blast from signature hole blasts can be used to estimate air blast from future production blasts.

Comparison of vibration on the pipeline and on ground surface provides reference relation for future vibration estimates from that measured on the ground surface.

Measurement of the frequency response from the signature hole vibration can be used for frequency shifting of production blasts.

Ground sonic velocity, multiple seed waveforms, and vibration attenuation law from signature hole blasts were obtained and form complete input to the MSW blast vibration model. With the MSW model, various design scenarios can be compared. The MSW modelling can assist the mine to control the blast vibration at the pipeline and the highwalls whilst maximising the blasting productivity.

Acknowledgements: Gaichang Zhao and John Shephard from Orica Canada Inc. are acknowledged for their technical assistance. Gordon Frost from Abacus Mining and Exploration and Scott Scovira from Orica USA Inc. are acknowledged for initiating the project.

References

Persson Per-Anders, Holmberg R. and Lee Jaimin, 1994, Rock Blasting and Explosive Engineering, CRC press, Boca Raton New York

Ruilin Yang and D. Scott Scovira, 2007, A Model For Near-field Blast Vibration Based on Signal Broadening and Amplitude Attenuation, Explo 2007, Australiasian Institute of Mining and Metallurgy, Woolongong, September 3-4.

Ruilin Yang, 2007, Near-Field Blast Vibration Monitoring, Analysis and Modeling, 33th Conf. Explosives and Blasting Technique, USA.

Ruilin Yang, James Gunderson, Tamara Whitaker , and Blake McMullin, 2008, A Case Study of Near-Field Vibration Monitoring, Analysis, And Modeling, Blasting and Fragmentation, Vol 2 Number 3.

Kay D. 2010, Summary of three eDev™ blasts fired at the Citybanan cross city railway project, Stockholm.

Yang R., and Scovira D. S., 2010, A model for near and far-field blast vibration based on multiple seed waveforms and transfer functions, *Blasting and Fragmentation,* 4(2), 91-116.

Yang, R., Scovira, D. S. and Patterson, N., 2009, An Integrated Approach of Signature Hole Vibration Monitoring and Modeling for Quarry Vibration Control, 9th International Symposium on rock fragmentation by Blasting, Spain 13-17 September 2009.

Yang, R. and Lownds, M. 2011, Modeling Effect of Delay Scatter on Peak Particle Velocity of Blast Vibration Using a Multiple Seed Waveform Vibration Model, 37th Conf. Explosives and Blasting Technique, San Diego, California, USA.

Appendix A
Estimate of ground sonic velocity from
the signal arrivals of vibration and air over pressure

The speed of the sound in air can be calculated as (http://en.wikipedia.org/wiki/speed_of_sound):

$$c_{air}(m/s) = 331.3\sqrt{1+\frac{\vartheta}{273.15^{o}C}} \quad (1)$$

where ϑ is the temperature in degrees Celsius (^{o}C).

Let ϑ=-5, c_{air}=328.26 m/s

Figure A1 shows a schematic view of paths of the blast vibration and air over pressure from a blast hole to a monitor station. It is assumed the blast vibration started from the primer of the charge and the air over pressure from the collar of the blast hole. The air over pressure started later than the blast vibration by a time delay (t_2 in Equation 2) for the detonation to propagate to the top of the charge and for the shock wave to the collar of the hole. The delay of the starting time (t_2) can be estimated from the velocity of the detonation, the charge length above the booster, and the shock wave velocity in the rock. In addition to the delay of the starting time, the air over pressure travels much slower than the ground vibration. Therefore, the arrival of the air blast signal in Channel #4 is delayed from the signal of the blast vibration (e.g. in Channel 1) by t_1.

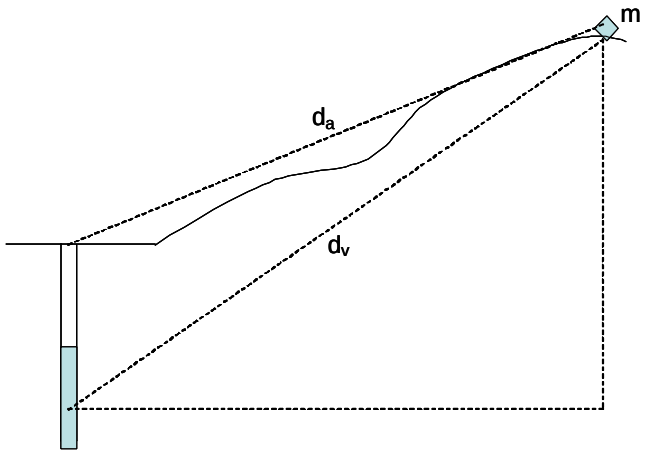

Figure A1. Schematic view of paths of the blast vibration and air over pressure from a blast hole to a monitor station

The following relationship exists:

$$\frac{d_a}{c_{air}} + t_2 = \frac{d_v}{c_{rock}} + t_1 \quad (2)$$

Where, d_a and d_v are the travel distances of air blast and blast vibration, respectively. c_{air} and c_{rock} are sound speed in air and rock.

Table A1. Ground sonic velocity (c_{rock}) calculation from signature holes of the Blasts #1 and #2

Hole #	dv (m)	da (m)	t1 (s)	t_2 (s)	crock (m/s)
Blast#1, Hole#1	296.2	294.6	0.8028	0.0021	3061.203
2	297.4	295.8	0.8047	0.00203	3020.977
3	297.8	296.29	0.8076	0.00191	3072.71
4	300.53	299	0.8115	0.00195	2966.342
5	302.44	300.92	0.8203	0.00195	3074.753
6	302.59	301.1	0.8193	0.00192	3029.514
7	288.75	287.04	0.8086	0.00207	4252.652
Blast #1 average					3210 m/s
Blast#2, Hole#1	513.12	511.8	1.3496	0.00203	2425.412
2	520.62	519.4	1.374	0.00193	2476.639
3	528.03	526.8	1.4335	0.00193	3047.696
4	540.11	538.9	1.499	0.00193	3734.775
5	546.46	545.3	1.5234	0.00187	3912.978
6	552.49	551.3	1.5371	0.002	3827.131
7	513.81	512.6	1.3906	0.00182	2973.66
Blast #2 average					3199 m/s

Table A1 displays the ground sonic velocity (c_{rock}) calculation from signature holes vibration and air blast recorded with Monitor #8 from the two blasts. It is assumed the shock wave in the rock and explosive charge to be 5000 m/s in the calculation. The average ground sonic velocity is calculated to be 3210 m/s for the Blast #1 and 3199 m/s.

It was expected that the sonic velocity of the second blast site should be lower than that from the first blast since the ground of the second blast is considered to be weaker. The difference in the ground sonic velocity from the two blasts in Table A1 is small.

Appendix B
Resonant frequency and frequency range that ground support (Yang et al, 2009)

From dynamics mechanics theory, a system with a single degree of freedom has one resonant frequency. A blast overburden or a site is a continuous deformable body (continuous system) and has infinite degrees of freedoms. Consequently, the overburden of a blast has infinite number of resonant frequencies. Practically speaking only the range (bands) of the resonant frequencies can be estimated. For a given ground condition, the range of the resonant frequencies may vary insignificantly for a relatively small change of the distance. A range of the resonant frequency may be used for an application.

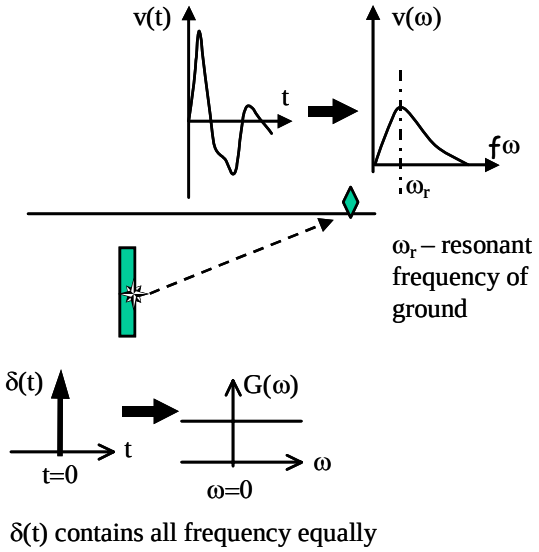

Figure B1. Sketch of the concept of using a single hole blast hole to estimate the resonant frequency of ground

The ground resonant frequency can be estimated using a single blast hole detonation as input to the ground and measuring the dominant frequency of the ground response - the frequency corresponding to peak amplitude. In this case, the input to the ground from the detonation of a single blast hole is approximated as a delta function in the time domain or as a function in the frequency domain of constant amplitude, as shown in Figure B1. The dominant frequency in this case can be considered as the resonant frequency of the ground.

The dominant frequency for a set of tri-axial vibration waveforms can be obtained from summation of Fast Fourier Transforms (FFT) of the tri-axial components of the particle velocity waveforms. In this way the relative contribution from each component is automatically taken into account. The dominant frequency is defined as the frequency at which the amplitude is the maximum over the whole frequency range (ω_r in Figure B1).

Ideally detonation from a spherical charge gives a better approximation of the delta function than a long cylindrical charge does. However, there is often a need to use signature hole vibration traces to model blast vibration from a production blast. The charge configuration of the signature hole blast is

selected to be typical of the loading for the production blast. Therefore, the estimate from the dominant frequency of a signature hole blast vibration provides an approximation of the ground resonant frequency.